Comparative study of Modeling a Hydrogen Nonpremixed Turbulent Flame

A. Obieglo, J. Gass, D. Poulikakos

Swiss Federal Institute of Technology - ETH
Mechanical and Process Engineering Department
Institute of Energy Technology
Laboratory for Thermodynamics in Emerging Technologies

accepted for publication

in Combustion and Flame, 2000

Type of article: full-length

Address of corresponding author:

Andreas Obieglo
LOW C2
ETH Zentrum
8092 Zürich
Switzerland
Tel. ++41-1-632 3645
Fax ++41-1-632 1023
e-mail obieglo@ltnt.iet.mavt.ethz.ch

Abstract

The topic of this work is the numerical simulation of a turbulent non-premixed hydrogen (H_2) jet-flame with different combustion models. The predictions are validated against existing experimental data provided by Raman and Laser Doppler Anemometry (LDA) measurements for a turbulent jet hydrogen-air diffusion flame ([1], [2]). In particular, a comparison of two "advanced" turbulent combustion models is presented: These are a Probabilistic Euler Lagrangian (PEUL) model based on the idea of Lagrange interaction by exchange with the mean (IEM) and a model based on the scalar probability density function (PDF) transport equation for the thermo-chemical variables which is solved using a Monte Carlo method. In addition a "standard" Eddy Dissipation model with a single-step reaction is considered. The numerical results for mean velocity components, turbulent kinetic energy, mixture fraction, temperature and major chemical species are presented and compared with the experimental data. The goal of the work is to investigate the capabilities of the used models in predicting hydrogen combustion in a jet-flame. This simple geometry allows for reliable flow simulations. Regarding the basic test case under consideration, the results obtained by the PEUL computations and the Monte Carlo simulation are in good agreement with experimental data. The comparison shows that both probabilistic methods give better predictions than the "standard" model. The advantages and disadvantages of the models are discussed in detail in relationship to the results. It is possible to draw conclusions for modeling improvements. The improved models should be able to be applied also to more complex geometries.

Nomenclature

A, B, C	model constants
D	diffusion coefficient
H	enthalpy
L	characteristic length
P	pressure
P_{pc}	Pope correction term
P_k	production term in ε equation
$\tilde{P}$	Probability Density Function, Favre averaged
Pr	Prandtl number
Pr_t	turbulent Prandtl number
S	chemical source term
Sc	Schmidt number
Sc_t	turbulent Schmidt number
T	temperature
Y	mass fraction
Z	mixture fraction
c	heat capacity
h	specific enthalpy
k	kinetic energy
r_j	stoichiometric coefficient of species j
t	time
u	velocity component
x	space coordinate

Greek Symbols

σ	number of elements
τ	characteristic time
ε	dissipation rate
λ	heat conductivity
μ	viscosity
μ_t	turbulent viscosity
ρ	density
ω	source term
Φ	scalar vector
Ψ	composition space vector

Subscripts

f	fuel
i,j	space direction
M	constant for IEM model
n	species
o	oxidizer
p	product
t	turbulent
α, β	element
ε	dissipation
$\varepsilon_{1,2,3}$	model constants
μ	model constant

Superscripts

-	time averaged
$\sim$	Favre averaged
.	production rate
"	fluctuation

1 Introduction

Rising computer power and better understanding of combustion processes make computational research in the area of combustion attractive. Several phenomena have to be taken into account. The field of combustion is divided into non-premixed and premixed combustion, whereas partial premixing is also playing an important role in bridging the gap between these limits. In the field of non-premixed turbulent combustion although much progress has been achieved in the last several years many questions are still widely discussed. Because of the complex interaction of chemical reactions and mixing processes, advanced models have been developed and applied [3], [4], [5], [6], [7], [8], [9].

Good model predictions can be used in construction of furnaces or gas turbines as well as for the prediction of pollutants such as nitrogen oxides. Since the development of the models is still continuing, a comparison between solution strategies will be helpful in providing insight to the advantages and disadvantages of the different approaches. This will facilitate the future selection of suitable models for specific applications.

The simplest geometries for producing turbulent, non-premixed flames, are a counterflow or a coflow configuration. Especially the coflow geometry has the advantage that the flow field can be predicted quite well with existing turbulence models ([10], [11], [12]). Furthermore, the boundary conditions can be defined very accurately, which is an important topic for the simulations. In both cases good optical access for measurements is possible. While the counterflow geometry is still a topic of discussion [7] a complete data set for the coflow geometry is available for hydrogen combustion ([1], [2]). Well defined sections through the flame render a comparison between simulation and experiment. The hydrogen flame of the present study belongs to a set of standard flames, which have been defined in a recent workshop [13].

The objective of this work is to compare different combustion models in order to investigate their capability to predict combustion processes. All models are applied to the calculation

of a well defined test-case. The simplified geometry allows concentration on the combustion modeling. Although the flow is turbulent, the predictions for the flow field are in good agreement with experimental data. In order to obtain a measure of how well the advanced models work in comparison to simpler standard models, an Eddy Dissipation Model was also employed.

The probabilistic Eulerian Lagrangian (PEUL) model is used in the Lagrange IEM (*Interaction by Exchange with the Mean*) concept. The model was developed by Borghi [14] and applied to methane combustion by Vervisch [15] and to hydrogen combustion by Schlatter [16].

For the mixture fraction an assumed β-PDF is applied whereas for the one reactive species which occurs only on three lines in mixture fraction space, a delta function is used. The effects of the assumed form of the probability density function have been investigated by Kent and Bilger [17]. They found out that the form has only little effect on the velocity and the conserved scalar mean fields but is more significant in determining mean temperatures and molecular species compositions, which is in agreement with our observations.

The molecular mixing is modelled with the interaction by exchange with the mean. A Lagrangian line based on a one-step mechanism in mixture fraction space, combined either with a line of mixing or with a line of fast chemistry close to chemical equilibrium, provides the values for the source term in the species transport equation.

The PDF-method used in the calculations is closely related to Pope's [18]. In our case an equilibrium assumption is applied for the fast hydrogen chemistry in the Monte Carlo calculation of the PDF transport equation. All chemical species can be expressed as a function of the mixture fraction. The density and the chemical species are obtained by interpolation from look-up tables. The mixing process is also modelled with the interaction by exchange with the mean model.

A flamelet model including preferential diffusion could also be interesting for this type of

flows as the model is taking diffusion effects into account, which play an important role on the nearfield region. On the other side, in regions further upstream, it might come to an overprediction of diffusion effects which could not be obtained in the experiment. In the work of Schlatter a flamelet calculation for two different strain rates has been discussed [16]. In this work the flamelet concept was not included.

The combustion models are applied in conjunction with a sophisticated commercially available code named CFX-TASCflow, which is used to solve the Navier-Stokes equations [19]. The code uses a Finite Volume method, based on the Finite Element approach. In our case the geometry is represented with a rectangle in the vertical plane of the flame. The standard $k-\varepsilon$ model was used. The examined flame is a turbulent non-premixed diffusion jet flame with inlet conditions of $Re = 10000$. Whereas the Eddy Dissipation Model is commonly implemented in commercial codes, the two probabilistic methods have been combined by our research team with CFX-TASCflow. The code for the the PEUL model is described more in detail in [16]. The PDF code has been developed as a result of a cooperation with the *Institute of Applied Computation, ICA,* at Stuttgart University and is described in more detail in [20].

The comparison includes mean values of the temperature and the main species. To the best of our knowledge direct comparison of a PEUL with PDF calculations of the hydrogen jet flame has not been published yet. The comparison allows identification of the advantages and disadvantages of both models as well as their performance compared to a "standard" model.

The article consists of four parts. Starting with the general description of the governing equations the turbulence modeling is discussed. The introduction of the three combustion models then follows. After a brief explanation of the hydrogen jet flame experimental setup the results together with a discussion are presented. The conclusion summarizes the findings of the presented work.

2 Problem definition and Modeling

Experimental setup of previous work ([21], [2])

The experimental setup consists of a vertical burning hydrogen jet with an exactly defined coaxial air stream as shown in figure 1. Its discussion will also serve to define geometrically the problem of interest.

The experiments have been performed by Barlow [21] for the temperature and the species concentrations and by Flury [2] for the flow field. The inner diameter of the tube is 3.75 mm, the outer is 4.8 mm. The air-velocity has been fixed at $1m/s$ for all measurements. The Reynolds number for the flame is 10'000 with 100% hydrogen in the fuel-jet. The vertical measurement area is a hexagonal wind channel with a diameter of 0.6 m and the length of 2 m. Two walls of glass allow optical access to the flame. The design of the wind channel in the experimental setup of [21] and [2] differs only slightly with no influence on the experiment. Combined LDA and CARS measurements at the Swiss Federal Institute of Technology showed that the two studies ([21], [2]) are in very good agreement, which allows usage of the data sets from both experiments indiscriminately.

The flame has a visible flame length of $675mm$. The computational domain has a size that can be resolved by a grid very well. It is also possible to define sections through the flame for comparisons as given in table a.1. The boundary condition of the inlet velocity profile is measured by adding particle tracers to the fuel jet. The geometry allows for good optical access at all flame levels.

The measurements of the mean and the variance of the velocity have been recorded at our laboratory with a three dimensional LDA, using seeding particles in the stream [2]. Radial measurements have been taken at 1/16L, 1/8L, 1/4L, 3/8L, 1/2L, 5/8L, 3/4 L, 1L, where L denotes the visible flame length. The positions are the ones used by Barlow [1]. The size of the probe volume is about $80\mu m$ [2].

The measurements are provided without error bars. Therefore the uncertainties will be mentioned in the text.

The temperature and species measurements of Barlow [1] have been obtained with Raman/Rayleigh/LIF. Measurements of the temperature, the mixture fraction, the species H_2, O_2, H_2O, OH and NO are reported. For a more detailed description [1], [13], [22] and [23] are recommended.

Combustion Modeling

A general conservation equation for a scalar can be written as:

$$\rho(\Phi)\frac{\partial \Phi_\alpha}{\partial t} + \rho(\Phi)u_i\frac{\partial \Phi_\alpha}{\partial x_i} = \frac{\partial}{\partial x_i}\left(\rho D\frac{\partial \Phi_\alpha}{\partial x_i}\right) + \rho(\Phi)S_\alpha(\Phi) \tag{1}$$

where Φ denotes all conserved scalars taken into consideration. Starting with this equation it is possible to derive a set of governing equations for mass, momentum, species and energy. In turbulent flows the mean chemical source term does not appear in closed form and therefore has to be modelled.

On the other hand, it is possible to derive a transport equation for a probability density function. This has the advantage of a closed source term. Nevertheless, new terms like the turbulent mixing still have to be modelled.

Both sets of governing equations will be presented in the following sections.

2.1 Favre averaged governing equations

The Favre averaged governing equations for mass, momentum, species mass fractions and enthalpy can be written in Cartesian coordinates as

$$\frac{\partial \bar{\rho}}{\partial t} + \frac{\partial \bar{\rho}\tilde{u}_j}{\partial x_j} = 0 \tag{2}$$

$$\frac{\partial \bar{\rho}\tilde{u}_i}{\partial t} + \frac{\partial \bar{\rho}\tilde{u}_i\tilde{u}_j}{\partial x_j} = -\frac{\partial \bar{P}}{\partial x_i} + \frac{\partial}{\partial x_j}\left\{(\mu + \mu_t)\left(\frac{\partial \tilde{u}_i}{\partial x_j} + \frac{\partial \tilde{u}_j}{\partial x_i}\right)\right\} \tag{3}$$

$$\frac{\partial \bar{\rho}\tilde{Y}_n}{\partial t} + \frac{\partial \bar{\rho}\tilde{u}_j\tilde{Y}_n}{\partial x_j} = \frac{\partial}{\partial x_j}\left\{\left(\bar{\rho}D_n + \frac{\mu_t}{Sc_t}\right)\frac{\partial \tilde{Y}_n}{\partial x_j}\right\} + \overline{\dot{\omega}}_n \tag{4}$$

$$\frac{\partial}{\partial t}\left\{\bar{\rho}\left(\tilde{H} - \frac{\bar{P}}{\bar{\rho}}\right)\right\} + \frac{\partial \bar{\rho}\tilde{u}_j\tilde{H}}{\partial x_j} = \frac{\partial}{\partial x_j}\left\{\lambda\frac{\partial \tilde{T}}{\partial x_j} + \frac{\mu_t}{\mathrm{Pr_t}}\frac{\partial \tilde{h}}{\partial x_j} + \sum_{n=1}^{N}\bar{\rho}\,D_n\,h_n\,\frac{\partial \tilde{Y}_n}{\partial x_j}\right\} - \sum_{n=1}^{N}h_n^f\,\overline{\dot{\omega}}_n \tag{5}$$

with $\bar{\rho}$ the mass density, $\tilde{u}_i$ the velocity vector components, $\bar{P}$ the pressure, λ the thermal conductivity, $\mathrm{Pr_t}$ the turbulent Prandtl number, D_n the mass diffusivity of species n, $\tilde{Y}_n$ the species mass fraction, $\overline{\dot{\omega}}_n$ the chemical production rate and μ and μ_t the laminar and turbulent dynamic viscosity, respectively. The $\sim$ denotes the Favre averaging and $\bar{}$ the time averaging. The *Lewis number* is assumed to be equal to unity for all species; therefore the mass diffusivity D_n of species n is assumed to be constant. Subsonic conditions (Low Mach number conditions) are assumed.

The mean total enthalpy is defined as:

$$\tilde{H} = \tilde{h} + \frac{\tilde{u}_i\tilde{u}_i}{2} + \tilde{k} \tag{6}$$

where $\tilde{k}$ represents the turbulent kinetic energy:

$$\tilde{k} = \widetilde{\rho u_i'' u_i''}/(2\bar{\rho}) \tag{7}$$

The static enthalpy $\tilde{h}$ is given by

$$\tilde{h} = \int_{T_0}^{T} c_p \, d\tilde{T} \tag{8}$$

where c_p, the specific heat coefficient at constant pressure, is assumed to be a function of temperature and composition.

Modeling of the turbulence

Turbulence is modelled with the standard $k-\varepsilon$ model [10], [11] and the turbulent dynamic viscosity is obtained from

$$\mu_t = C_\mu \, \bar{\rho} \, \frac{\tilde{k}^2}{\tilde{\varepsilon}} \tag{9}$$

In case of the jet flame, a correction is necessary to predict the correct spreading rate of a round jet. This is performed by using the Pope correction P_{pc} [12] as an additional term in the equation for ε:

$$\frac{\partial(\bar{\rho}\tilde{\varepsilon})}{\partial t} + \frac{\partial(\bar{\rho}\tilde{u}_j\tilde{\varepsilon})}{\partial x_j} = \frac{\partial}{\partial x_j} * \{(\mu + \frac{\mu_t}{\sigma_\varepsilon}\frac{\partial\tilde{\varepsilon}}{x_j})\} C_{\varepsilon 1}\frac{\tilde{\varepsilon}}{\tilde{k}} P_k - C_{\varepsilon 2}\bar{\rho}\frac{\tilde{\varepsilon}^2}{\tilde{k}} + P_{pc} \tag{10}$$

where the Pope correction is given as

$$P_{pc} = C_{\varepsilon 3}\frac{\tilde{\varepsilon}^2}{\tilde{k}} S_\varepsilon \tag{11}$$

The source term in cylindrical coordinates can be written as

$$S_\varepsilon = \frac{1}{4}\left(\frac{\tilde{k}}{\tilde{\varepsilon}}\right)^3 \left(\frac{\partial\tilde{u}_x}{\partial r} - \frac{\partial\tilde{u}_r}{\partial x}\right)^2 \frac{\tilde{u}_r}{r} \tag{12}$$

The constant $C_{\varepsilon 3} = 0.79$. The standard model constants have been chosen.

The chemical source term is computed via combustion models described in the following sections.

2.2 The Eddy Dissipation Combustion Model

The EDM was introduced by Magnussen [24] and its usage has become widespread in industrial applications. The combustion model is based on the following single step reaction:

$$\text{fuel} + r_j \text{oxidizer} \leftrightarrow (1 + r_j) products$$

The basic assumption of this widely used model is fast, irreversible, one-step chemistry. Because of the fast chemistry assumption, the combustion is determined by the turbulent mixing process. In other words, there is no coupling between chemical reaction and turbulent mixing. Complete chemistry means that at the end of a reaction the stoichiometric species mass fraction of fuel or oxidizer are totally consumed. The chemical source term for the transport equation has then the following form:

$$\overline{\dot{\omega}}_f = -\mathrm{A}\ \bar{\rho}\ \frac{\tilde{\varepsilon}}{\tilde{k}}\ \mathbf{min}\left\{\tilde{Y}_f, \frac{\tilde{Y}_o}{r_f}, \mathrm{B}\frac{\tilde{Y}_p}{1 + r_f}\right\} \tag{13}$$

where A and B are empirical constants. In our case the standard values A = 4 and B = 0.5 are applied.

Boundary conditions

The mean inlet velocity of the fuel jet is $296\frac{m}{s}$ with an error of ± 1.5 %. The Reynolds-number of the inlet stream was 10000. Data obtained in [2] for the velocity and the turbulent kinetic energy profiles measured closed to the nozzle exit were utilized as boundary conditions. For

the dissipation rate ε no measurements are available. This rate was estimated with the formula for the turbulent length scale:

$$\varepsilon = \frac{k^{3/2}}{L_\varepsilon} \tag{14}$$

For the integral length scale L_ε the inner radius of the nozzle was used. The air coflow is entering with a mean velocity of $1\frac{m}{s}$ which is assumed to have a smooth profile within an error of about 1.3 % over the radius. A symmetry boundary condition is taken on the axis of symmetry. The computational domain consists of a rectangle. At the outlet region constant atmospheric pressure is assumed. For the other nodes which are not fixed by boundary conditions, an arbitrary distribution of fuel, oxidizer and products is assumed for the first iteration.

2.3 The PEUL Combustion Model

PEUL stands for *Programme Eulerien Lagrangien* or *Probabilistic Euler Lagrange* which accounts for the Eulerian calculation of the flow field, e.g. the convection and the diffusion with Lagrangian tracking of a fluid particle to describe the chemical reaction.

The PEUL model provides a PDF for a species mass fraction, namely oxygen, conditioned on the mixture fraction. The averaged source term then can be calculated from

$$\overline{\dot{\omega}}_{O_2} = \int_0^1 \left[\int_0^1 \dot{\omega}_{O_2}(Y_{O_2}|Z) P(Y_{O_2}|Z) dY_{O_2} \right] P(Z) dZ \tag{15}$$

The PDF of the mixture fraction is represented by a presumed $\beta - PDF$ based on the mixture fraction and its variance. The conditional PDF is represented by a δ-function described in equation (18).

In the Lagrangian description, the development of the mass fraction due to mixing and chemical reaction may be described by

$$\frac{\partial Y_i}{\partial t} = \frac{(\tilde{Y}_i - Y_i)}{\tau_t} + \dot{\omega}_i \tag{16}$$

A transformation of equation (16) in mixture fraction space yields

$$\frac{\partial Y_i}{\partial Z} = \frac{(\tilde{Y}_i - Y_i) + \tau_t \dot{\omega}}{\tilde{Z} - Z} \tag{17}$$

where Y_i denotes the mass fraction of species i, Z the mixture fraction, $1/\tau_t$ the exchange frequency where τ_t is assumed to be proportional to the turbulence time ($\sim$ describes a Favre averaged value). In the PEUL model, O_2 is taken as species for the mass fraction.

The equation describes the motion of a reacting fluid particle and its mixing process in the composition space.

Depending on the mixing time τ_t, three different regions can be defined and described, taking into account the different time scales. For large Damkohler-numbers, where time scales for mixing are large compared with the chemical time scale, chemical equilibrium exists. All mass fractions Y_i are lying on the equilibrium line in the composition space. These states can be calculated directly. With fast mixing and slow reaction it is a pure mixing process. The states can be calculated from equation (16) for $\tau_t \to 0$. For the states between those two limits the local time scale $\tau_t \approx \tilde{k}/\tilde{\varepsilon}$ will be considered.

The development of the mass fraction of oxygen in mixture fraction space in the PEUL model is given for three different time scales which leads to three lines for the species mass concentration in mixture fraction space: one line is the limiting case of pure mixing where the source term is set to be zero. The other limitation in mixture fraction is described for fast chemistry. The chemical source term is then calculated from the flame sheet model which is based on the chemical equilibrium. The third line lies between those two limits. In this case the source term in equation (17) is obtained by a reduced one-step mechanism for

hydrogen combustion. A two-step reduced mechanism is applied only for the determination of the oxygen mass fraction on this line [16] .

Which lines are chosen to calculate the source term depends on the averaged mass fraction $\tilde{Y}_{O_2}$ as a progress variable compared to the mass fraction of the Lagrangian line. Only two lines are taken, always including the Lagrangian line. In regions of fast chemistry, which occur at most locations of a hydrogen flame, the results of the PEUL modelled source term are close to chemical equilibrium. Only close to the nearfield at the nozzle the distribution differs from equilibrium states [16]. It is a main idea of the model to have the chemistry described as a mixture of two lines in mixture fraction space.

The conditional PDF $P(Y_{O_2}|Z)$ is set at every point zero except on the three lines and it can be described as

$$P(Y_{O_2}|Z) = \sum_{l=1}^{3} \alpha^l \delta(Y_{O_2} = Y_{O_2}^l(Z)) \tag{18}$$

where l denotes one of the three lines and α the value of the δ-PDF. The values of the weighting coefficients α can be found from three conditions: The summation over the three coefficients is equal to one, the integration over the mass fractions of the three lines for oxygen weighted with the joint PDF should yield the mean value $\tilde{Y}_{O_2}$ and either the probability density for the fast chemistry line or the line of pure mixing is set to zero. For more details we refer to [16] and [15]. Therefore only the Lagrangian line with the fast chemistry or the Lagrangian line with the mixing line describes the chemical behaviour. In most regions of the flame (except for x/L = 1/8), the chemistry is closer to chemical equilibrium which determines the use of the Lagrangian line together with the fast chemistry. Under these conditions it seems to be justified to compare the chemistry in the PEUL model with the assumption of chemical equilibrium used in the PDF transport equation.

The PEUL model is coupled with an Eulerian flow solver.

Boundary conditions

The same boundary conditions as in case of the EDM calculations were used. The initial guess is based on the results of the EDM simulation.

2.4 PDF-transport equation

Starting with a general transport equation for a conserved scalar (equation 1), it is also possible to derive a transport equation for the probability density function. The one-point PDF is given then by the following governing equation:

$$
\begin{aligned}
&\frac{\partial}{\partial t}\langle\rho\rangle\tilde{P} = \\
&- \frac{\partial}{\partial x_i}\langle\rho\rangle\tilde{u}_i\tilde{P} \\
&- \frac{\partial}{\partial x_i}\langle\rho\rangle\langle u_i'' \mid \Phi = \Psi\rangle P \\
&+ \frac{\partial}{\partial x_i}\left(\langle\rho\rangle D\frac{\partial}{\partial x_i}\tilde{P}\right) \\
&- \langle\rho\rangle\frac{\partial}{\partial\Psi_\alpha}\frac{\partial}{\partial\Psi_\beta}\left[\langle D\frac{\partial\Phi_\alpha}{\partial x_i}\frac{\partial\Phi_\beta}{\partial x_i} \mid \Phi = \Psi\rangle\tilde{P}\right]
\end{aligned}
\tag{19}
$$

The density weighted form of the PDF $\tilde{P}$ is chosen because of the strong density fluctuations in a reacting flow. The ensembles for turbulent mixing are denoted with α and β.

For the mixture fraction as a conserved scalar the source term disappears. Except for the nearfield region of x/L = 1/8 where non-equilibrium effects occur, the fast hydrogen chemistry is close to equilibrium ([1], [16]).

The statistical distribution due to turbulent mixing and chemical reactions in the flow field is described with a one-point PDF $\tilde{P}(\Psi_1, \Psi_2, ...; \mathrm{x}, t)$ of the thermo-chemical variables $\Phi_1, ..., \Phi_n$, where (Ψ_i) is a composition variable and (Φ_i) the appropriate variable of the probe space [18]. The attributes of the turbulent flow field have been described by a standard $k-\varepsilon$ turbulence model. The density is calculated by the PDF-equations to close the flow field

model [20].

The turbulent convection is modelled by a gradient diffusion model:

$$\langle\rho\rangle\langle u_i'' \mid \Phi = \Psi\rangle\tilde{P} \cong -\frac{\mu_T}{Sc_T}\frac{\partial\tilde{P}}{\partial x_i} \tag{20}$$

The turbulent mixing is based on a relaxation process of the local distribution towards the mean values and modelled with Dopazo's IEM Model [25].

$$\left(\frac{\partial\tilde{P}}{\partial t}\right)_{turb.Mix.} \cong -\frac{1}{2}\frac{C_M}{\tau_t} * \frac{\partial}{\partial\Psi_\alpha}\left(\Psi_\alpha - \langle\Phi_\alpha\rangle\right)\tilde{P} \tag{21}$$

where C_M denotes the constant of the mixing model which is set equal to two and τ_t stands for the turbulent time scale and is calculated by

$$\tau_t = \frac{\tilde{k}}{\tilde{\varepsilon}} \tag{22}$$

Therefore, the mixing rate is given only by local values of the flow field without information about larger scales of the turbulent field. In addition to the influence of turbulence, the influence of combustion must also be taken into account in order to account for the interaction between turbulence and combustion. The lack of these two factors could result in errors. As a first approach the calculations have been carried out for nine species, using the equilibrium assumption. This implies that only the mixture fraction as the only scalar will be transported in the transport equations [26], [27].

Boundary conditions

The same boundary conditions as in case of the EDM calculations are used. The initial guess is based on the results of the EDM simulation. Radiation effects have been neglected

in the calculations. The heat loss due to radiation of pure Hydrogen combustion might have an influence on the temperature peak. Therefore this topic will be investigated in future.

3 Results

The velocity profiles for a reacting flow are calculated for all three combustion models with the $k-\varepsilon$ model and round jet correction by Pope [12]. Due to safety considerations, no measurements of a cold hydrogen jet flow were carried out. Cold flow data are available for a nitrogen jet. Calculations for the cold flow with the $k-\varepsilon$ model and Pope-correction have been provided by Schlatter [16] and show very good agreement with experimental data. Therefore the use of those models is a good choice for calculating the flow field.

The physical domain of the computational grid in radial direction is 33 times the radius of the nozzle with 51 nodes, and in axial direction, it has the length of the visible flame which is given by $675mm$ with 251 nodes. For the computation of the flow fields for all three cases a grid with about 40000 nodes is used. Even though the computation is performed in 2D, the solver for the flow field requires at least three cells in the third direction, setting periodic boundary conditions at the interfaces. In the inlet region as well as toward the center line, the grid is refined. A comparison of the flow field with a grid of 66000 nodes showed no significant difference in the obtained data. Therefore grid independence of the calculation with the coarser grid was demonstrated.

In our study simulations are compared at different downstream positions with experimental data. Figure 2.a shows the normalized flow field of the EDM calculation and figure 2.b is the flow field obtained in the PEUL calculation. The flow field related to the PDF calculation is presented in figure 2.c . The velocity values are normalized with the velocity on the centerline. Radial distance is normalized with the radius of the jet nozzle. All three calculations give good agreement with experimental data which allows for further comparison of chemistry and turbulence interaction. It can be seen that the turbulence model together with the round jet correction are a good choice for modeling the jet flow. Only at position x/L = 1/8 for a radial distance between 5 and 10 times R_{Fuel} do the results for the flow field in all three computations give a slightly larger spreading than experimental data. This points

to some difficulties of the turbulence modelling in handling the steep density gradients in regions of high turbulence. The two constants for the Eddy Dissipation Model have been set to A = 4.0 and B = 0.5 according to their common use in most applications. A variation of the constants has been performed with only very little difference on the flow field. It could be seen that with the above values, the model comes closest to experiment. The good prediction of the flow-fields justifies for a detailed comparison of the different combustion models.

Turbulent Kinetic Energy

Data of turbulent kinetic energy are provided for the inlet boundary condition [2]. They are used as inlet conditions for the calculations. The turbulence intensity for the air coflow is given within 10 % [2]. In figure 3.a the results of the Eddy Dissipation Model case are presented. The results for the PEUL and the PDF modeling are very closely related to the one presented. Close to the center axis *at x/L =1/8*, the simulation overpredicts the values for k for all three models. Modelling of the turbulence in regions with strong density gradients in the turbulent flow field at high velocities could cause the differences. Preferential diffusion, which occurs especially in the inlet region, may also influence the kinetic energy field. None of the models takes these diffusion effects into consideration. Further downstream the agreement is quite good as shown in figures 3.b, 3.c. and figure 3.d (x/L = 1). For this flame the qualitative distribution is predicted correctly in all profiles. The chosen $k-\varepsilon$ - model with the Pope round jet correction leads to a useful modeling of the flow field.

Mixture fraction distribution

For the mixture fraction the definition of Bilger is applied [28] based on the hydrogen and oxygen element mass fractions. The stoichiometric value of the mixture fraction is 0.028. In figure 4.a (nozzle exit) all models except for the PDF calculation slightly underpredict the experimental data at the center axis. All three models overpredict the mixture fraction between 5 and 10 r/R_{Fuel} which corresponds to the behaviour of the flow field in this region

and therefore can be addressed to the modelling of turbulence. Effects of preferential diffusion in the nearfield region of the nozzle exit may also play a role. This trend persists in figures 4.b and 4.c (further downstream) only for the PEUL model which indicates an influence of the combustion modelling on the mixing process not observed in experiment. In figure 4.d (x/L = 1) the PEUL model is also close to experimental data, whereas the PDF computation slightly underpredicts the mixture fraction. The uncertainties of the measurements of the mixture fraction based on calibration flames are 5.1 % . The computation of the velocity field for the PDF, PEUL and EDM calculation corresponds to the prediction of the mixture fraction as a conserved scalar. The comparison shows generally good agreement of calculated data with experiment which allows for a more detailed comparison of species and temperature.

Mass fraction of Y_{H_2}

The behaviour of the Y_{H_2} mass fraction distribution is similar to that of the mixture fraction. In figure 5.a all models, except of the PDF calculation, underpredict the maximum on the center axis and slightly overpredict the experimental data for r/R > 5. This trend is followed only by the PEUL model in figures 5.b and 5.c (further downstream). In the PDF calculation of figure 5.c, half of the available hydrogen according to the experimental data is already consumed. This may be a result of equilibrium chemistry leading to a faster reaction in the nearfield of the nozzle compared to experiment, whereas in the PEUL modelling due to the additional Lagrangian line, more hydrogen is left over. Note that the mixture fraction for x/L = 1/2 is slightly overpredicted in the PEUL calculation. The EDM simulation underpredicts only slightly the experimental hydrogen distribution. The reason may be related to the behaviour of the model which burns down the educts very quickly. In figure 5.d (x/L = 1) all models correspond with the experiment where no fuel is left.

Mass fraction of Y_{O_2}

In the plots of the oxygen radial distribution at the axial position of figure 6.a (near the bottom of the flame), all three models predict an oxygen consumption closer to the air

side than the experimental data. Notice that none of the models take into account effects of preferential diffusion. This phenomenon together with super-equilibrium of OH can be observed in the region of x/L = 1/8 [1]. According to the conditional plots for hydrogen and oxygen (figures 9) non-equilibrium chemistry is dominating in this region. Both phenomena have influence on the flame structure, and therefore make it difficult for correct prediction. The maximum of the temperature (the temperature distribution will be discussed in detail subsequently), which is correlated to the flame front in the experiments is closer to the side where most of the oxygen is already consumed. The combustion models predict the temperature maximum at the region where about half of the oxygen is consumed. It can be seen that this region corresponds with an overprediction of the mixture fraction for all models. The high turbulent density gradients at high inlet velocity causes difficulties for the modelling of turbulence. In figures 6.b (x/L = 3/8) and 6.c (x/L = 1/2) the Eddy Dissipation model is coming very close to predicting the correct oxygen mass fraction. The PDF and PEUL calculations are in very good agreement with the experiment. Further downstream at x/L = 1/1, figure 6.d, the PEUL and the Eddy Dissipation model slightly underpredict the existing oxygen mass fraction and the PDF method predicts about a third higher mass fraction, which corresponds to the results of the mixture fraction. It is reported from experiments that preferential diffusion plays only minor role in these regions. The chemistry is closer to equilibrium. This corresponds to the assumption of chemical equilibrium in the PDF calculation. In the PEUL model one of the three lines in mixture fraction space is the line of chemical equilibrium. Note that in case of the Eddy Dissipation Model the computation is based on mean values whereas in the PDF-Transport and the PEUL model, a PDF is applied which allows the coexistence of unburned fuel and oxidizer at the same location and time.

Mass fraction of Y_{H_2O}

In the case of the water mass fraction, the production rate at the inlet region in figure 7.a is also closer to the air side, and the maximum at 5 r/R_{Fuel} is slightly underpredicted by all

three models. This observation is in agreement with to the results for the mixture fraction in this region and shows that the turbulence modelling and the non-equilibrium has the most influence on this region. Neither the effects of preferential diffusion nor super-equilibrium states have been taken into account. In figures 7.b (x/L = 3/8 and 7.c, x/L = 1/2) the PDF transport and the EDM calculation show good agreement with experimental data. The slight underprediction in the PDF calculation may come from a point where chemical equilibrium is achieved earlier. In case of the PEUL calculation, the line for chemical equilibrium is combined with the Lagrangian line which leads finally to higher production of water. In the case of the EDM computation, the predicted maximum is at the same position as in the experiment. At the end of the flame in figure 7.d the production of water is underpredicted by the PDF method and slightly overpredicted by the PEUL and the EDM model, which corresponds to the results of the mixture fraction computation.

Temperature-profiles

The temperature profiles in the hydrogen flame illustrate a changing behaviour as one moves downstream along the axis. In the region close to the nozzle exit in figure 8.a, all three models have their temperature maximum shifted closer to the oxygen (air) side relative to the experiment. It is the region where the interaction of chemistry and turbulent mixture can not be predicted correctly due to the modelling of turbulent mixing. Non-equilibrium chemistry and effects of preferential diffusion may also play an important role. In the middle region of the flame, figures 8.b and 8.c, the the PEUL model is still closer to the oxygen side, where the PDF model predicts the experimental data very well. The results for the Eddy Dissipation in this region overpredict the temperature over the whole radial line, whereas the position of the maximum temperature is in agreement with experimental data. In the end region of the visible flame in figure 8.d the temperature predictions of the EDM and PEUL models are too high even when a radiation model is applied in case of PEUL model [16]. In the PDF model the predictions are too low although no radiation model is applied. The state of chemical equilibrium might be earlier achieved than in experiment and therefore

the flame length would be reduced. The slight overprediction of the mixture fraction in this region leads to high temperatures.

Note that in all the models at the x / L = 1 position (figure 8.d) the hydrogen is totally consumed. However, in the PDF model the hydrogen is consumed closer to the nozzle exit than in the PEUL model (see also figure 5.c). This may be influenced by the equilibrium assumption which implies fast chemistry. The comparison of PDF shapes (figure 11.d) shows only at this position a higher probability for lower temperature in case of the PDF transport modelling compared to experimental results. In the PEUL model two lines for describing the chemistry in mixture fraction space are taken into consideration: additionally to the line for chemical equilibrium the Lagrangian line, based on a reduced mechanism. This may lead to a better prediction. The production rate reproduces the chemical time scale in the nearfield of the nozzle more accurately. Further downstream the experiment is close to chemical equilibrium. The temperature profiles in the middle section are predicted quite well by the PDF modelling; in this case the underprediction of H_2 has no influence on the temperature due to the fact that there is still enough hydrogen to burn. It is worth recalling that in our case radiation is neglected and the fuel is assumed to be incompressible.

Conditional plots of X_{O_2} *and* H_2

The conditional means of the mole fractions of oxygen and hydrogen are plotted in figure 9. This gives the possibility to study the chemistry of the turbulent flow in mixture fraction space. The results for equilibrium chemistry, the Eddy Dissipation results and experimental data are plotted against mixture fraction. Additionally in figure 9.a additionally the Burke-Schumann line for hydrogen is included which indicates how close equilibrium chemistry is related to the limit of fast chemistry. Only around stoichiometry one can observe differences. In figures 9.b,9.c and 9.d the line of chemical equilibrium is very close to experimental data. Therefore the assumption of equilibrium chemistry in the PDF and PEUL computation is well justified. Only at position x/L = 1/8 can small differences around stoichiometry

be observed, which indicates effects of non-equilibrium chemistry. The high inlet velocity in this region causes high turbulence. In the reacting flow high gradients of density and temperature occur with strong impact on the flow field. The Eddy Dissipation Model for all positions around stoichiometry predicts higher values of oxygen and hydrogen, which means that the reaction rate in the Eddy Dissipation Model is too low.

Note that the results for the equilibrium chemistry indicates that in case of the PEUL model most time the Lagrangian line is combined with the line of chemical equilibrium. The differences in the mean values could therefore be attributed to the additional Lagrangian line and different shapes of the PDFs.

Conditional plots of the temperature

The conditional plots for the temperature are plotted in figure 10. At x/L=1/8 (figure 10.a) an underprediction of the temperature can be observed for the Eddy Dissipation Model which corresponds to the overprediction of hydrogen and oxygen in mixture fraction space (figure 9.a). The assumption of chemical equilibrium at this position, which is applied in the PDF transport as well as in on PEUL line, leads to a higher maximum in temperature. This indicates the non-equilibrium behaviour of chemistry in this region. The differences between the two maximum temperatures is reduced at positions further downstream (figures 10.b, 10.c and 10.d). In these regions the Eddy Dissipation Model is also overpredicting the maximum temperature between a few up to 50 Kelvins. The differences may be caused by some radiation effects which are not taken into account for the equilibrium chemistry and the Eddy Dissipation model. It can be observed, that radiation has only little influence on the temperature in our case. It can be seen that the assumption of chemical equilibrium for these regions is well justified.

Conditional temperature PDFs

From experiment as well as from the PDF-Transport computation scatter-plot data for all nodes have been available. In figure 11 conditional temperature PDFs are presented for

a mixture fraction range between 0.05 and 0.105 . The non-uniform shape of the PDFs gives an impression of the different forms which can be obtained at several positions. It can be seen, that the shapes of the PDFs in figures 11 a, b and c are in good agreement with experimental data. This corresponds to the results obtained in physical space for the temperature. Only at the downstream position x/L = 1/1 one can observe a different location of the positions of the maximum: in case of the PDF-transport modelling lower temperatures have a higher probability than it is the case in experiment. This problem might be addressed to the prediction of turbulent mixing. In experiment there is still a probability of reaction with high temperatures. The combustion process seems to be already finished in the PDF-computation.

4 Conclusions

A hydrogen jet flame with $Re = 10000$ was studied numerically. Experimental data of existing studies ([1], [2]) obtained by LDA, Raman, Rayleigh and LIF measurements have been utilized for comparisons. For the combustion modeling a PEUL Model, a Monte Carlo solution of a PDF transport equation and an Eddy Dissipation Model were considered. The flow field was calculated with the standard $k - \varepsilon$ model which was extended with the *Pope correction*. The simulations of the flow field provided a good agreement with experimental data. Therefore differences in the results were attributed to the combustion modeling.

The Eddy Dissipation Model has the advantage of being relatively inexpensive and simple to use. The calculated data in physical space were mostly in agreement with the experiments except for temperature discrepancies that occurred in mixture fraction space. This is mostly related to the fact that the chemistry in the Eddy Dissipation method is dominated by mixing using a global one-step reaction and that no probabilistic distribution is taken into account.

The PEUL and the PDF method showed mostly good agreement with experimental data. Even with the simple chemistry approach can reasonably good predictions be made. The methods use large amounts of CPU-time, especially the PDF-transport modeling. The deviations from the experimental data at some locations may come from uncertainties of the turbulent mixing model and the simplification of the chemistry. Another effect might be the influence of radiation. In mixture fraction space the results with the assumption of chemical equilibrium are close to experimental data.

Taking into consideration the growing computer capability, which allows for faster computing at lower prices in the future, the PDF approach seems to be the most powerful modeling concept. For current calculations the PEUL model is a good alternative to the simple Eddy Dissipation Model which is used mostly in industrial applications.

For a more detailed insight, especially for the prediction of pollutants such as NO and NO_2,

a more detailed description of the chemical processes seems to be necessary. Therefore an extension of the modeling towards this direction is planned.

Acknowledgement

The authors would like to thank Rob Barlow and Matthias Flury for providing the measurements of the species and temperature and Martin Schlatter for providing results of the PEUL calculations. The work was supported by the *Swiss Department of Energy*, BFE.

References

[1] Barlow, R.S., and Carter, C.D. *Combust. Flame*, 97:261 (1994).

[2] Flury, M., and Schlatter, M., (1997). Technical report, http://www.ltnt.ethz.ch/combustion/nox/nox.html, ETH Zurich.

[3] Saxena, V., and Pope, S.B. *Twenty-Seventh Symposium (International) on Combustion*, The Combustion Institute, Pittsburgh, 1998.

[4] Subramaniam, S., and Pope, S.B. *Combust. Flame*, 115:487 (1998).

[5] Wouters, H.A., (1998). PhD thesis, TU Delft.

[6] Nooren, P., (1998). PhD thesis, TU Delft.

[7] Barlow, R., Chen, J.-Y., Bilger, R., Hassel, E.P., Janicka, J., Masri, A., Peeters, T., Peters, N., and Pope, S.B.,. *Third International Workshop on Measurement and Computation of Turbulent Nonpremixed Flames*, Boulder, 1998.

[8] Peters, N. *Prog. Energy Combust. Science*, 10:319 (1984).

[9] Chen, J.-Y., Chang, W.-C., and Koszykowski, M. *Combust. Sci. Technol.*, 110:505 (1995).

[10] Jones, W.P., and Launder, B.E. *J. Heat Mass Transfer*, 15:301 (1972).

[11] Launder, B.E., and Spalding, D.B. *Comp. Methods in Appl. Mech. and Engineering*, 3:269 (1974).

[12] Pope, S.B. *AIAA Journal*, 16:279 (1978).

[13] Barlow, R., and Carter, C.D. *Combust. Flame*, 104:288 (1996).

[14] Borghi, R. *Prog. Energy Combust. Science*, 14:245 (1988).

[15] Vervisch, L., (1996). PhD thesis, Universtiy of Rouen.

[16] Schlatter, M., (1996). PhD thesis, ETH Zürich.

[17] Kent, J.H. and Bilger, R.W. *Sixteenth Symposium (International) on Combustion*, The Combustion Institute, Pittsburgh, 1976.

[18] Pope, S.B. *Prog. Energy Combust. Science*, 11:119 (1985).

[19] ASC. *TASCflow User Documentation.* Advanced Scientific Computing Ltd. Waterloo, Ontario, 1996.

[20] Laxander, A., (1996). PhD thesis, Universität Stuttgart.

[21] Barlow, R.S. Sandia H2/He Flame Data - Release 1.1. Technical report, Sandia National Laboratories, Livermore, 1997.

[22] Flury, M., (1998). PhD thesis, ETH Zürich.

[23] Schlatter, M., Ferreira, J.C., Flury, M., and Gass, J. *Twenty-Sixth Symposium (International) on Combustion*, The Combustion Institute, Pittsburgh, 1996.

[24] Magnussen, B.F. and Hjertager, B.H. *Sixteenth Symposium (International) on Combustion*, The Combustion Institute, Pittsburgh, 1976.

[25] C. Dopazo. *Physics of Fluids*, 18:4 (1975).

[26] Kee, R.J., Rupley, F.M., and Miller, J.A. *Sandia Report*, SAND87-8215B, Livermore, 1992.

[27] Kee, R.J., Rupley, F.M., and Miller, J.A. *Sandia Report*, SAND89-8009B, Livermore, 1993.

[28] Bilger, R.W. *Twenty-Second Symposium (International) on Combustion*, The Combustion Institute, Pittsburgh, 1988.

List of Tables

x [mm]	x/L [-]
0	0
42	1/16
84	1/8
169	1/4
253	3/8
338	1/2
442	5/8
506	3/4
675	1/1

Table 1: *Absolute and normalised values of axial positions. L denotes the visible flame length.*

List of Figures

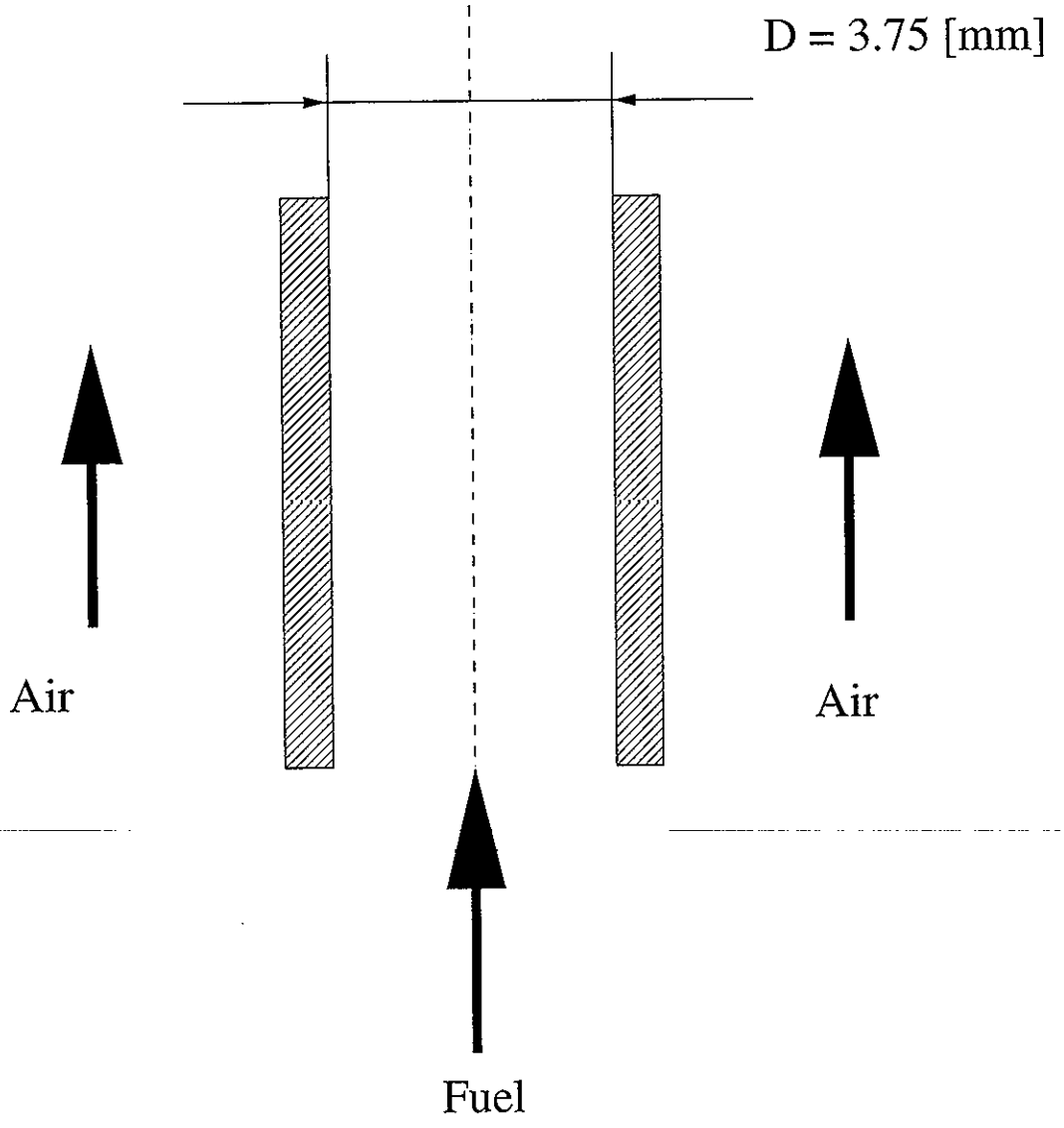

Figure 1: *Scheme of the nozzle for the jet-flame. The inner diameter is* $D = 3.75$.

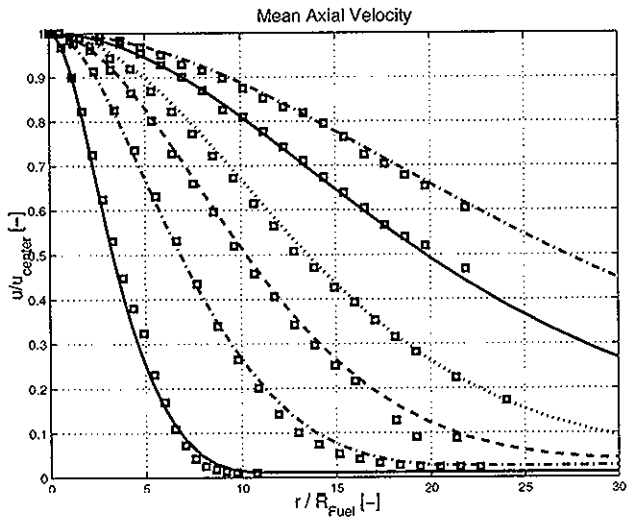

2.a $k-\varepsilon$ and EDM

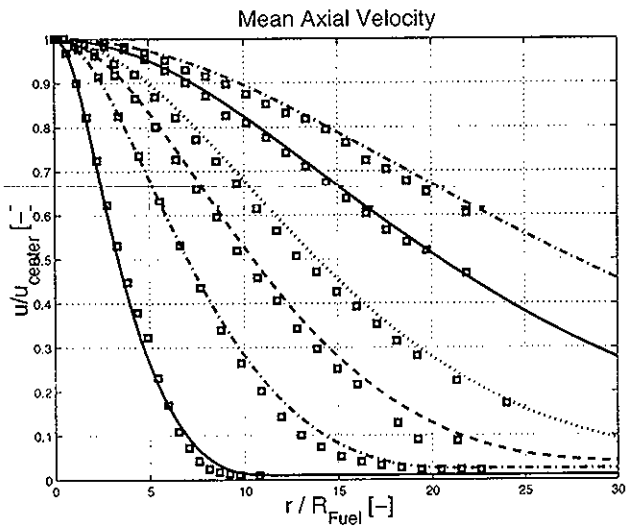

2.b $k-\varepsilon$ and PEUL

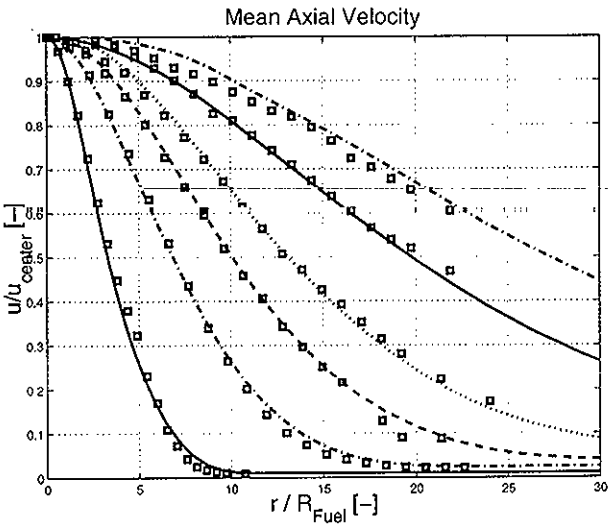

2.c $k-\varepsilon$ and PDF

Figure 2: *Normalized velocity profiles of the flow; (-) x/L = 1/8, x/L = 3/4; (-.-) x/L = 1/4, x/L = 1/1; (- -) x/L = 3/8; (...) x/L = 1/2; (o) Exp.*

figure 2

A. Obieglo,

J. Gass a

D.

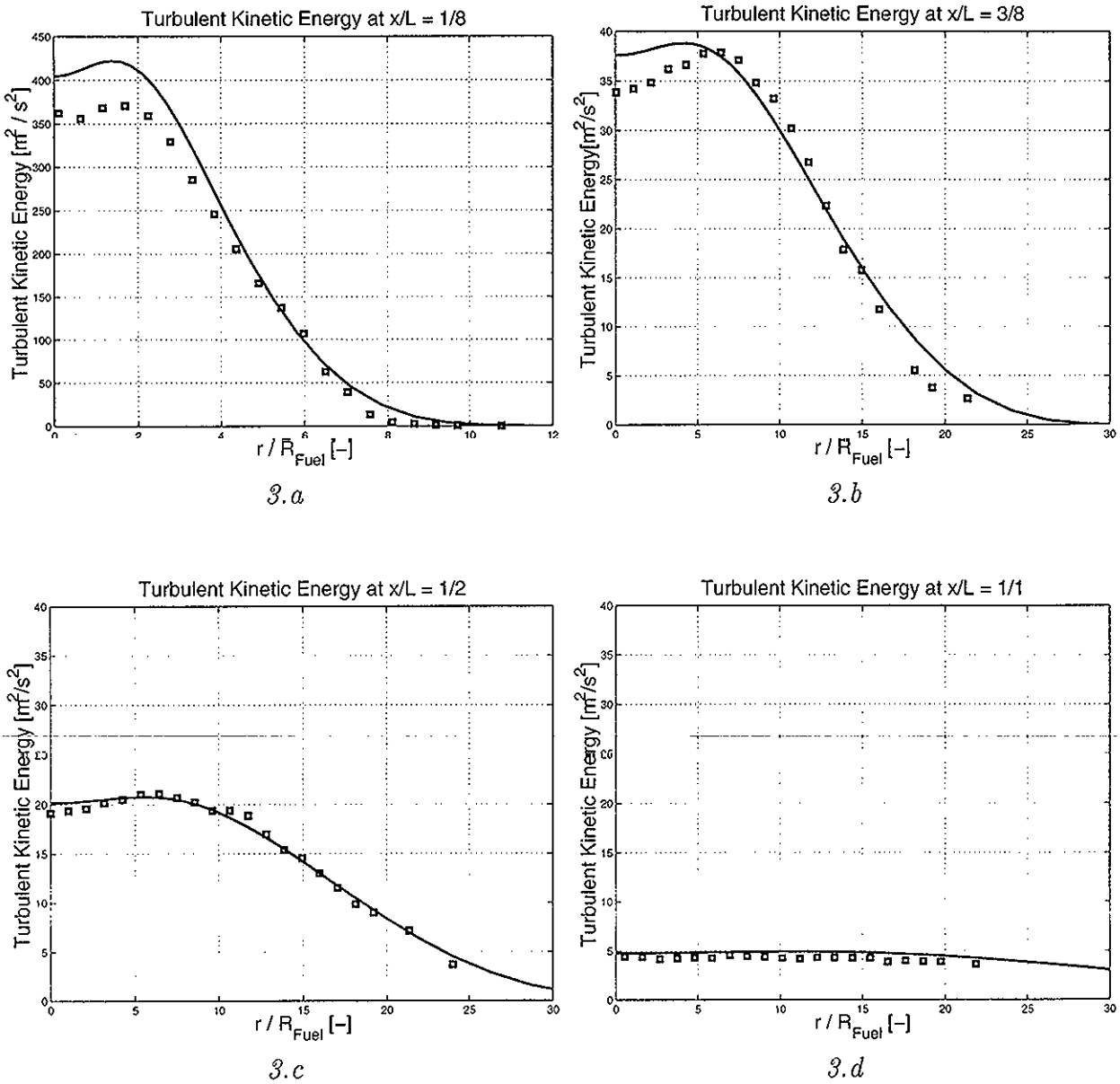

Figure 3: *Profiles of the Turbulent Kinetic Energy at four different downstream positions (–) simulation; (o) experiment*

figure 3

A. Obieglo,

J. Gass a

D.

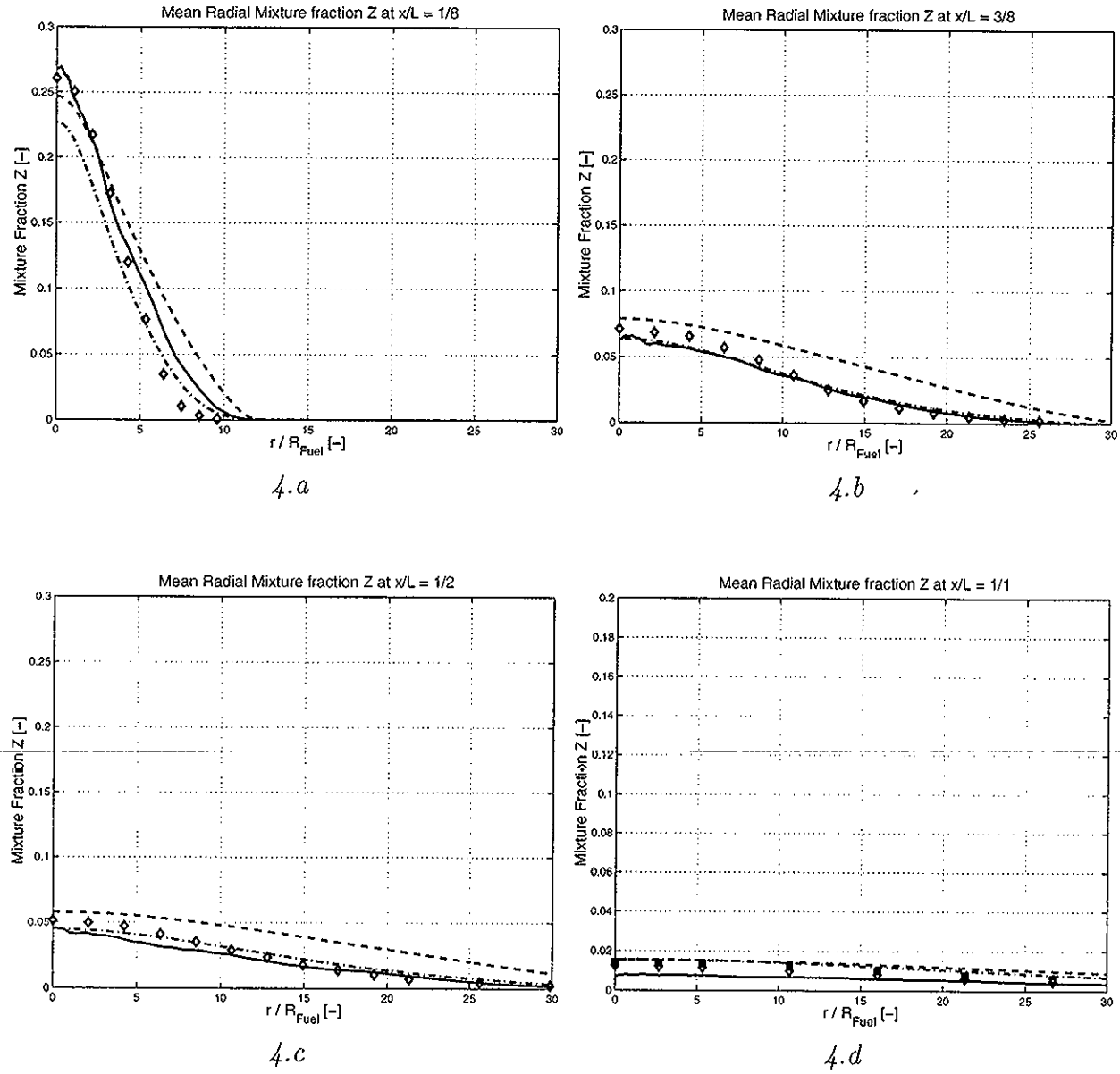

Figure 4: *Mixture Fraction Profiles at four different downstream positions; (-) PDF-transport; (-.-) Eddy Dissipation; (- -) PEUL; (◇) Exp. Fav. ave.*

figure 4

A. Obieglo,

J. Gass a

D.

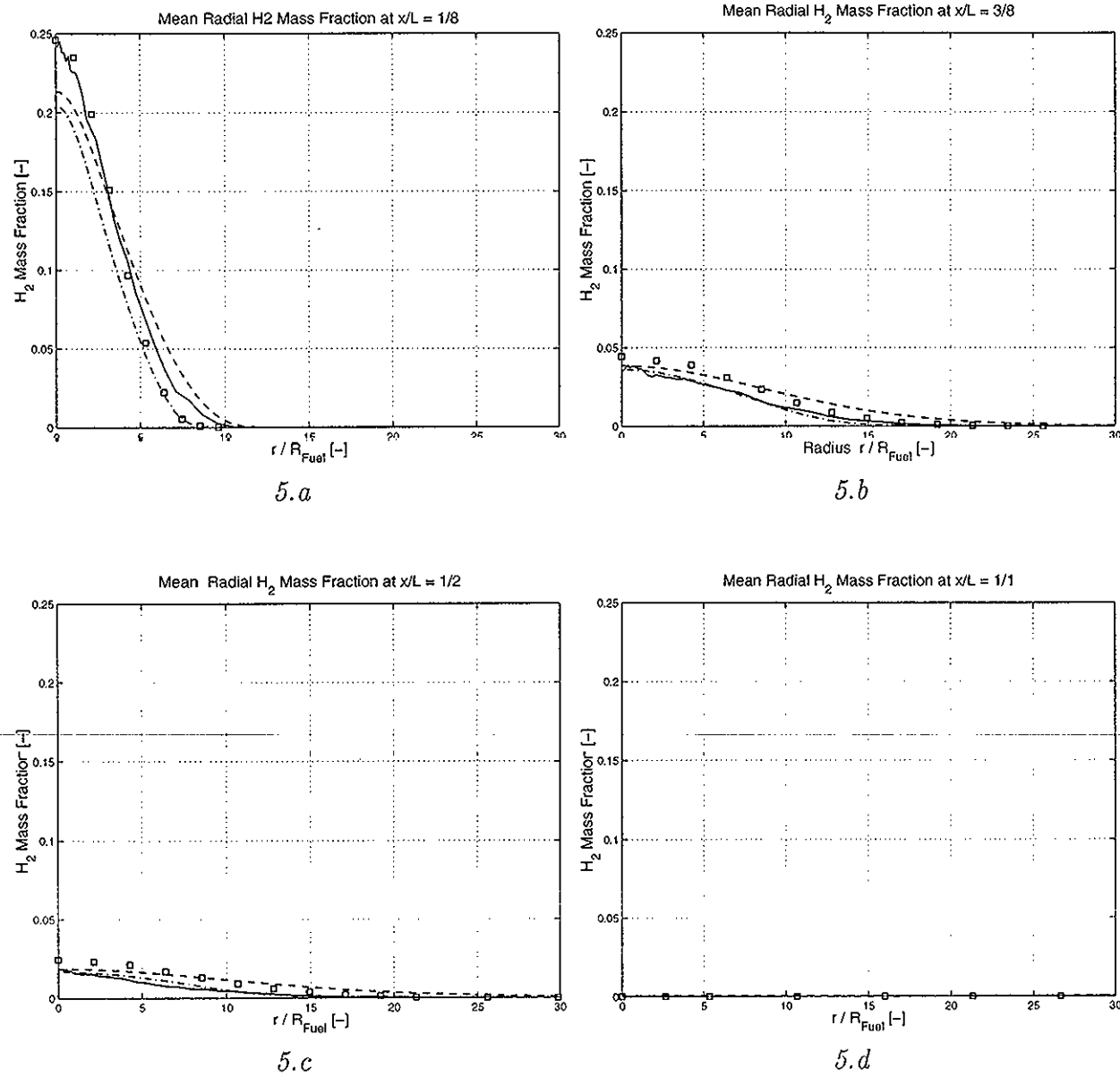

Figure 5: *Profiles of the mass fraction of Y_{H_2} at four different downstream positions (-) PDF-Transport;(-.-) Eddy Dissipation; (- -) PEUL; (o) Experiment*

figure 5

A. Obieglo,

J. Gass a

D.

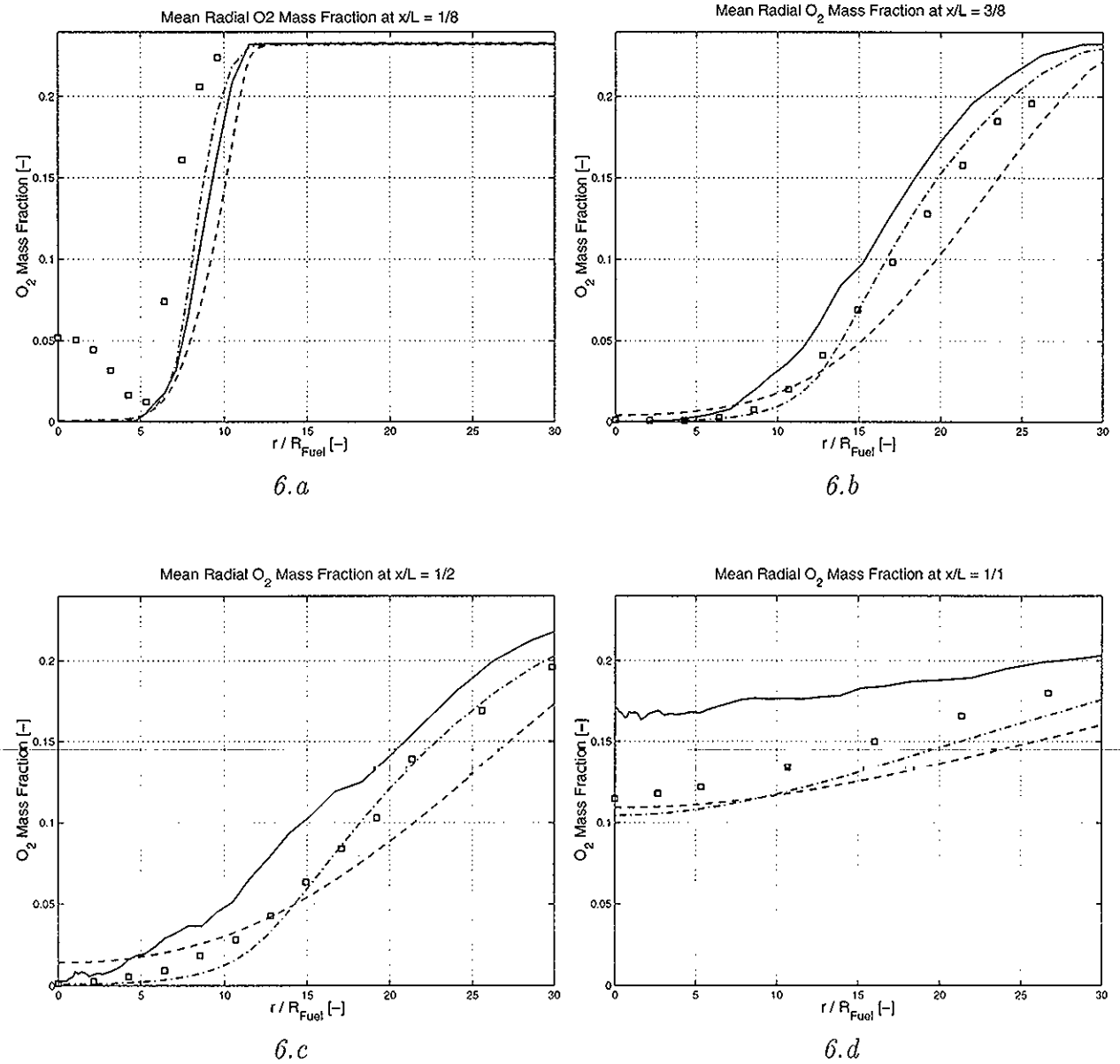

Figure 6: *Profiles of the mass fraction of Y_{O_2} at four different downstream positions (-) PDF-Transport;(-.-) Eddy Dissipation; (- -) PEUL; (o) Experiment*

figure 6

A. Obieglo,

J. Gass a1

D.

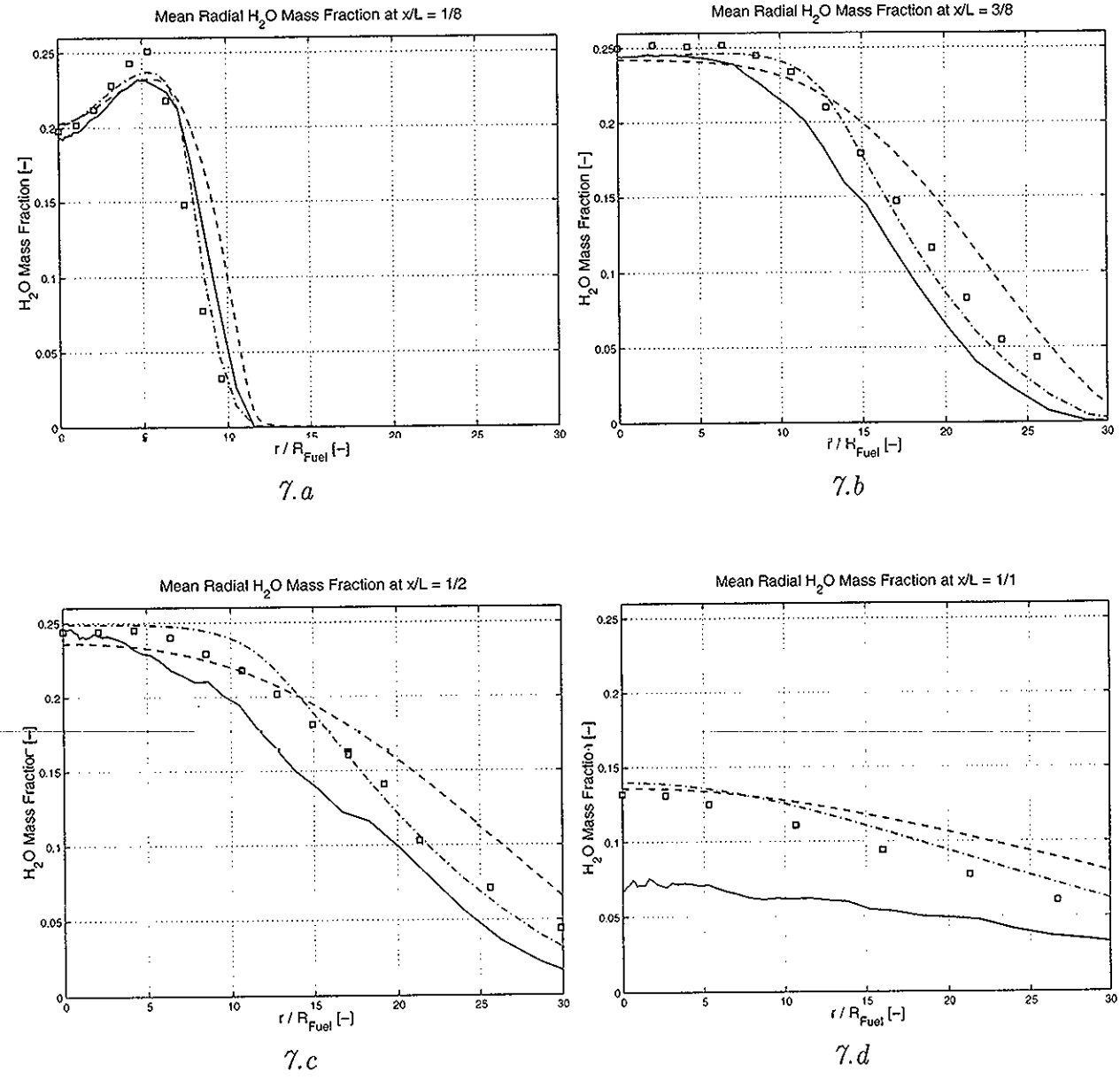

Figure 7: *Profiles of the mass fraction of Y_{H_2O} at four different downstream positions (-) PDF-Transport;(-.-) Eddy Dissipation; (- -) PEUL; (o) Experiment*

figure 7

A. Obieglo,

J. Gass a

D.

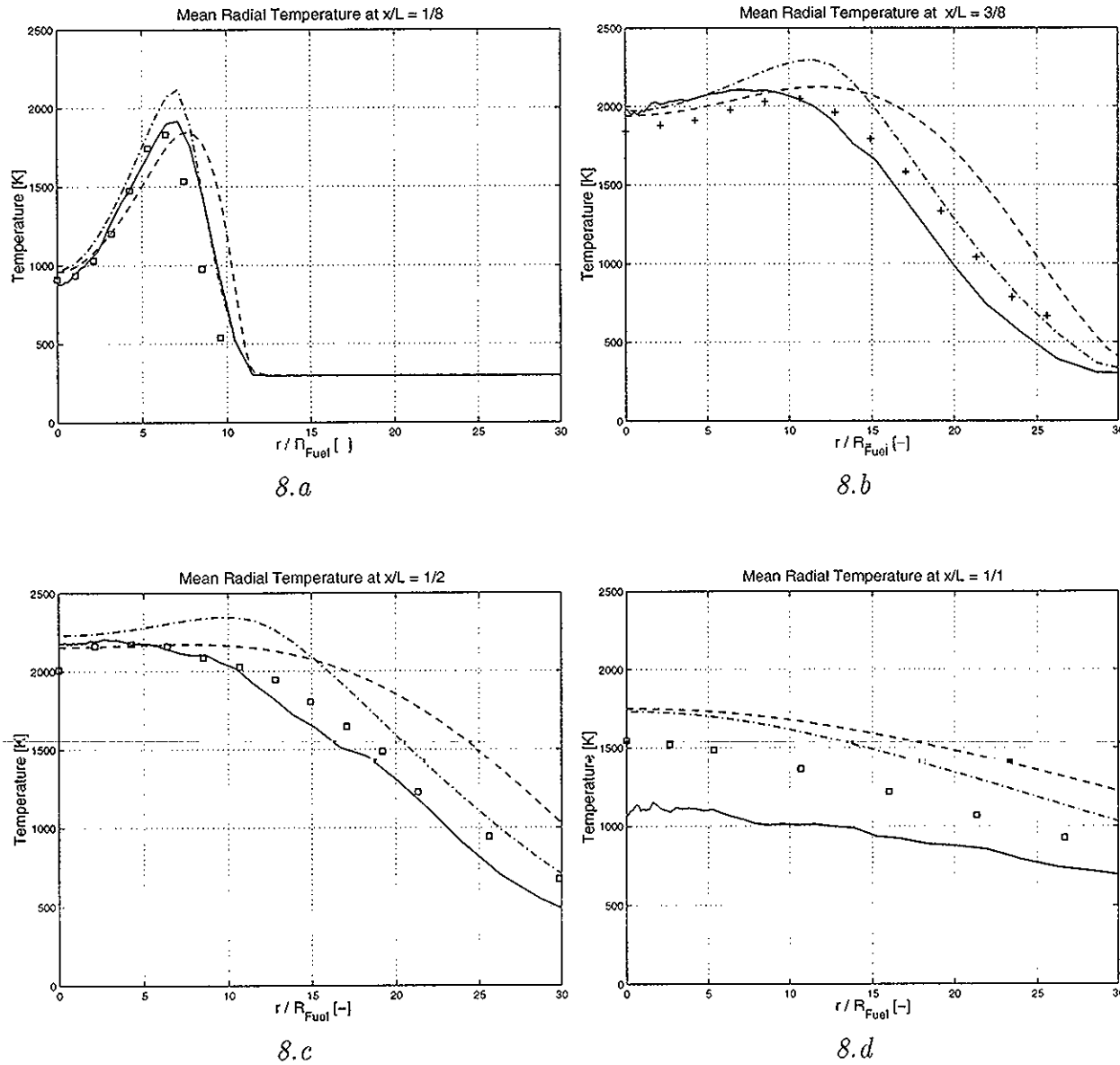

Figure 8: *Temperature Profiles at four different downstream positions (-) PDF-Transport;(- .-) Eddy Dissipation; (- -) PEUL; (o) Experiment*

figure 8

A. Obieglo,

J. Gass a

D.

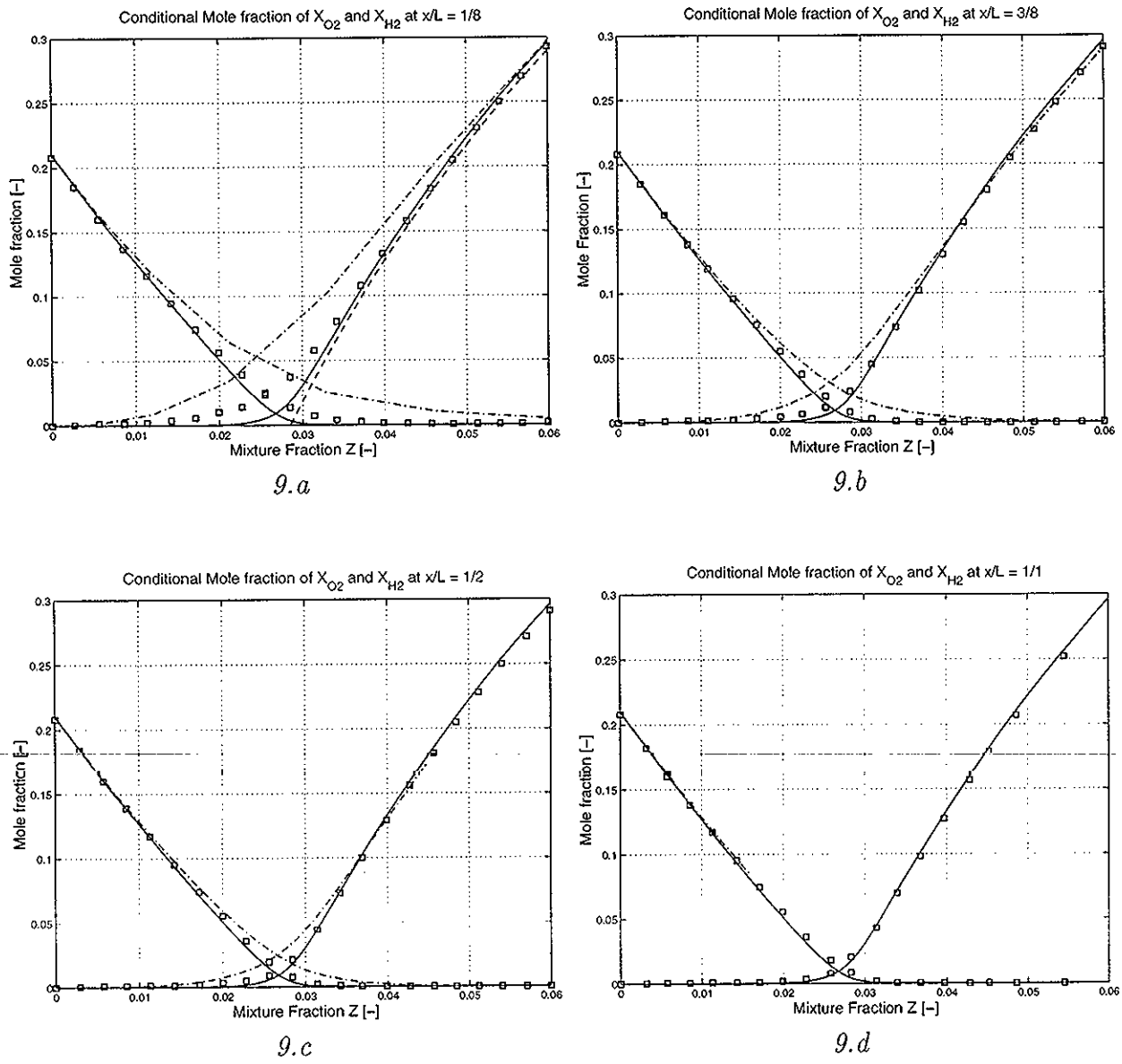

Figure 9: *Conditional Mole fraction profiles of hydrogen and oxygen at four different downstream positions; figure a) includes additionally the Burke-Schumann-line for hydrogen (- -). (-) Equilibrium chemistry;(-.-) Eddy Dissipation; (o) Experiment*

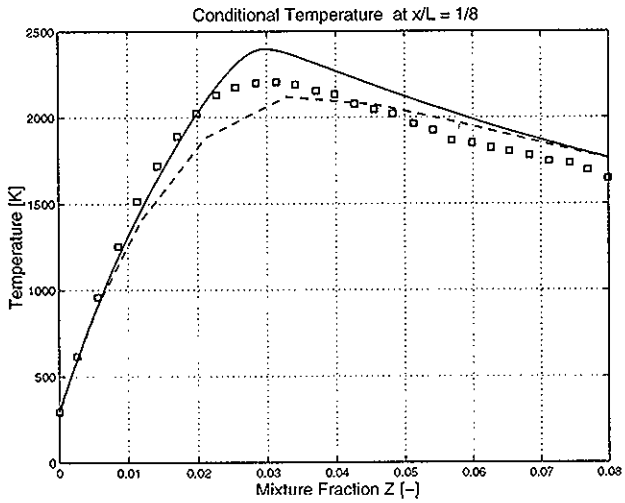

10.a

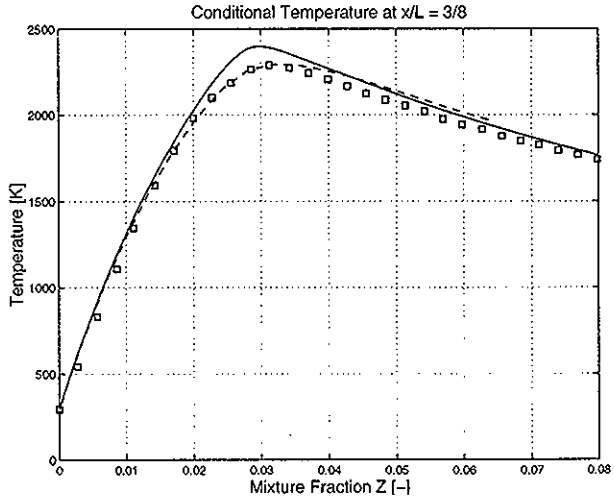

10.b

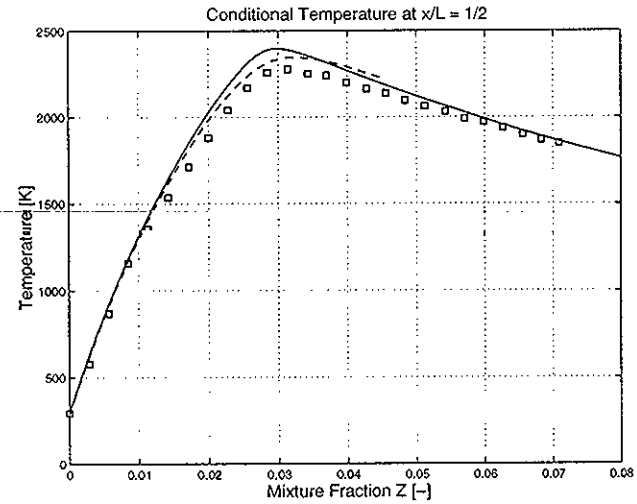

10.c

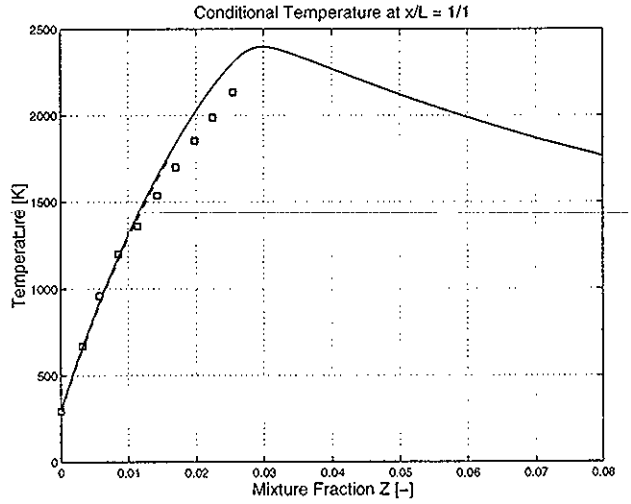

10.d

Figure 10: *Conditional Temperature Profiles at four different downstream positions (-) PDF-Transport;(-.-) Eddy Dissipation; (- -) PEUL; (o) Experiment*

figure 10

A. Obieglo,

J. Gass a

D.

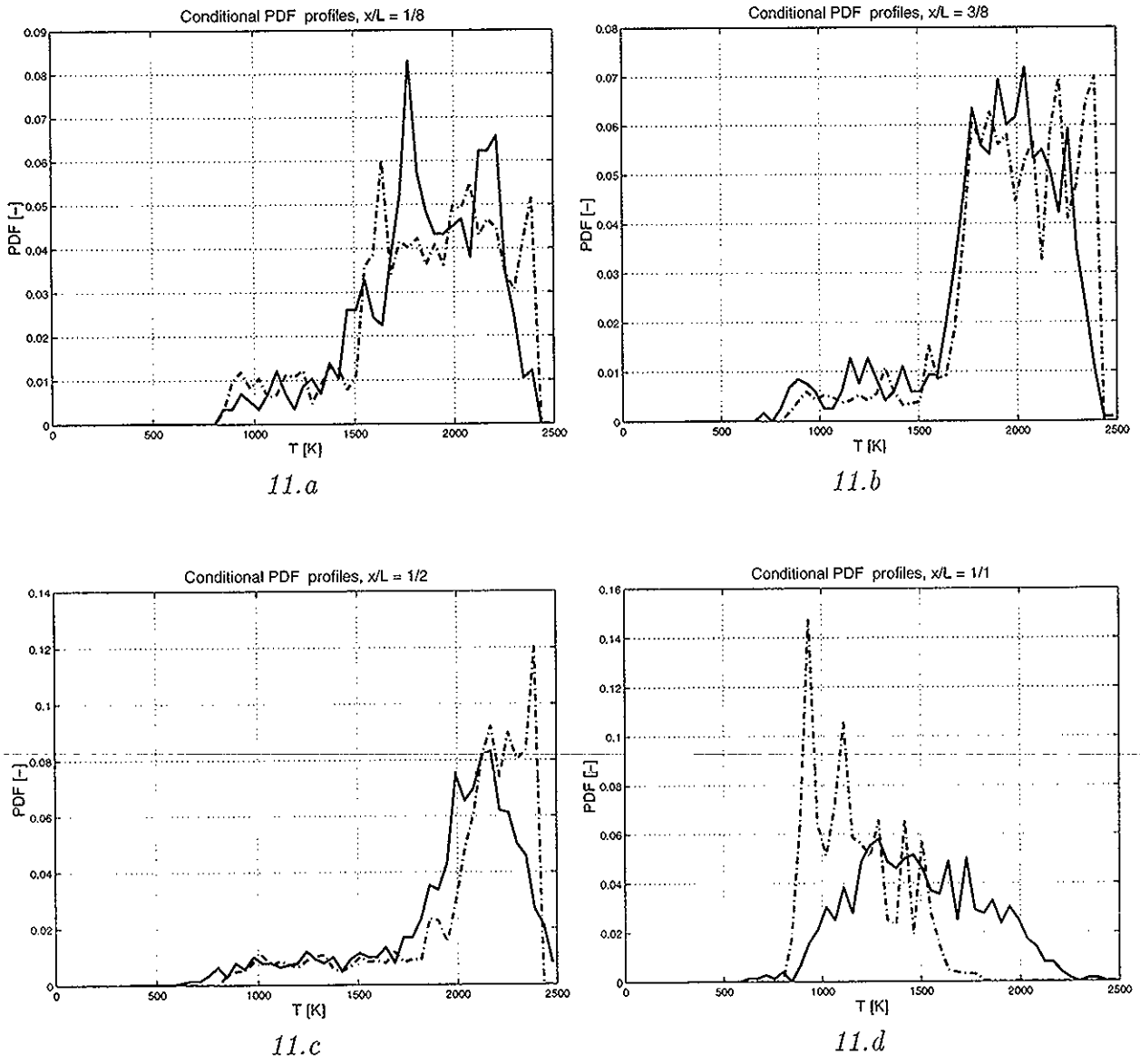

Figure 11: *Conditional Temperature PDFs at four different downstream positions from PDF-Transport. Mixture Fraction range between 0.05 and 0.105. (-.-) PDF-Transport; (-) Experiment*

figure 11

A. Obieglo,

J. Gass a

D.